Photodiagnosis and Photodynamic Therapy 38 (2022) 102796

Contents lists available at ScienceDirect

Photodiagnosis and Photodynamic Therapy

journal homepage: www.elsevier.com/locate/pdpdt

Triple-negative breast cancer treatment in xenograft models by bifunctional nanoprobes combined to photodynamic therapy

Viviane Paula dos Santos Jesus [a], Paula Fonseca Antunes Vieira [a], Ricardo Cesar Cintra [b], Luciana Barros Sant'Anna [c], Denise Maria Zezell [d], Maiara Lima Castilho [e], Leandro Raniero [a,*]

[a] Nanosensors Laboratory, Research and Development Institute, University of Vale do Paraíba, UNIVAP, Av. Shishima Hifumi, 2911, Urbanova, São José dos Campos, São Paulo 12244-000, Brazil
[b] Biochemistry Department, Universidade de São Paulo, USP, São Paulo, Brazil
[c] Histology and Regenerative Therapy Laboratory, Research and Development Institute, University of Vale do Paraíba, UNIVAP, São Paulo, Brazil
[d] Energetics and Nuclear Research Institute, IPEN, Universidade de São Paulo, USP, São Paulo, Brazil
[e] Bionanotecnology Laboratory, Research and Development Institute, University of Vale do Paraíba, UNIVAP, São Paulo, Brazil

ARTICLE INFO

Keywords:
Photodinamic therapy
Breast cancer
Photosensitizer
Nanoparticle

ABSTRACT

Triple-negative breast cancer (TNBC) overexpresses the Epidermal Growth Factor Receptor (EGFR), a characteristic of different types of tumors, linked to worse disease prognosis and risk of recurrence. Conventional treatments are also aggressive and can be morbid.. Therefore, t improvement and development of new methods are notorious. Photodynamic Therapy (PDT) is an effective method for treating different types of cancer by using light radiation to activate a photosensitizing agent (drug) in molecular oxygen presence, promoting cell death., Improving drug uptake in target cells could contribute to PDT efficiency. Accordingly, we developed a bifunctional nanoprobe (BN), used in PDT as a a treatment method *in vivo* against breast cancer. The BN uses gold nanoparticles with active targeting through the Epidermal Growth Factor (EGF) protein and Chlorine e6 (Ce6) carriers. We evaluated the therapeutic efficacy of *in vivo* xenograft in 4 groups: Saline, BN, Ce6+PDT, and BN+PDT. As a result, we observed that the BN+PDT group exhibited an excellent effect with greater selectivity to tumor tissue and tissue damage when compared to the Saline, BN, and Ce6+PDT groups. The results indicate a potential impact on breast cancer treatment *in vivo*.. In conclusion, our data propose that the BN developed heightened PDT efficacy through cellular DNA repair effects and tumor microenvironment.

1. Introduction

Breast cancer is a disease with high incidence and mortality in women worldwide [1]. It is a highly heterogeneous disease, which pathology classifies into molecular subgroups with different characteristics based on the expression of breast cancer receptors: estrogen receptor (ER), progesterone receptor (PR), and human epidermal growth factor receptor type 2 (HER-2) (1-3). ER, PR and HER-2 expression's absence classifies an aggressive breast cancer subtype: triple-negative breast cancer (TNBC) that is responsible for 10 to 20% of invasive breast cancer [2,5].

TNBC in general exhibits tumor hypoxia with necrosis and central fibrosis, which in turn promotes proliferation and metastasis [4,6]. Developing hypoxia favors tumor heterogeneity, stimulating aggressive growth, which genetically alters tumor cells, allowing them to get used to oxygen and nutrient deprivation [7,8]. TNBC has an overexpression level of Epidermal Growth Factor Receptor (EGFR) accelerating cell growth and carcinogenesis, due to acting on the regulation of cell proliferation, differentiation, migration, and survival [6]. In addition, there are few alternatives for treatments since it does not respond to hormonal therapy or therapies directed to receptors [2,3].

Thus, alternative therapies have been studied, such as Photodynamic Therapy (PDT), which is widely used to treat diseases as well as different types of tumors with promising therapeutic results in oncology. PDT can also be used in conjunction with other therapies, increasing the performance of the treatments.

In this context, EGF is an excellent approach to biomarker studies and PDT can be a choice for TNBC treatment using a powerful photosensitizer (PS) [9,10,11]. In our previous work, a new PS for PDT was designed to bind to the EGFR, increasing specificity and treatment

* Corresponding author.
E-mail address: lraniero@univap.br (L. Raniero).

https://doi.org/10.1016/j.pdpdt.2022.102796
Received 21 January 2022; Received in revised form 16 February 2022; Accepted 2 March 2022
Available online 6 March 2022

efficiency. The bifunctional nanoprobe (BN) was composed of gold nanoparticles, modified EGF, and Chlorine e6 (Ce6). Ce6 is one of the most used second-generation photosensitizers in PDT, known to generate reactive oxygen species ROS under light activation at biological optical window [15].

Nanoparticles (NPs) also provide active targeting by binding to receptors, heightening PDT selectivity, increasing effectiveness, and minimizing toxicity [12]. Tumor cells endocytic NPs, activated by irradiation, generating oxygen in tissues that convert to ROS. ROS causes hypoxia, cell death, and tumor destruction in response to PDT, which can be repeated without resistance. Tumors are damaged by apoptosis, a programmed cell death mechanism, where tumor cells undergo biochemical and morphological changes [13]. Thus, the tumor tissue presents limited oxygenation, expressing greater aggressiveness, consequently reducing the therapeutic response (chemotherapeutic and radiotherapy). Therefore, it is necessary to evaluate new methods to adjust treatment strategies better [14].

Aiming at the need for new treatments against TNBC, this study proposes to evaluate the antitumor and toxicological action of PDT using BN *in vivo*, which is the second part of the preview's work. For this purpose, TNBC cells (MDA-MB-468) were grown as xenografts in athymic nude mice, and we monitored their response to PDT.

2. Materials and methods

2.1. Animals and experimental groups

This study was approved by the Ethics Committee on Animal Use of University of Vale do Paraíba (protocol no. A07/CEUA/2018), and the animals were donated by Energetics and Nuclear Research Institute at São Paulo. Thirteen female eight-week-old BALB/c Nude Immunodeficient mice, with initial body weight of 20 g, were randomly divided into Saline (control), BN, Ce6+PDT, and BN+PDT groups. After fifteen days of adaptation period, the group saline (control group) included mice not xenografted, administrated with saline solution (0,9% mg/kg), and not submitted to PDT treatment ($n = 2$). Group Ce6+PDT represents mice xenografted, administrated with Ce6 (2 mg/kg) and submitted to PDT treatment ($n = 4$). Group BN+PDT represents mice xenografted, administrated with BN (2 mg/kg), and submitted to PDT treatment ($n = 4$). Group BN included xenografted mice that did not receive any drug administration and were not submitted to PDT treatment ($n = 4$). Mice were housed in polypropylene plastic cages with food and water *ad libitum*. Cages were maintained at a controlled temperature room (24 ± 2 °C) and cycles of 12:12 h, light and dark.

2.2. Xenografts and animals clinical evaluation

Animals were sedated with ketamine (10 mg/kg) (Dopalen, Ceva, Brazil) and xylazine (80 mg/kg) (Calmiun, Agener União, União Química, Brazil). Asepsis was executed at the injection site. The xenografts were performed by subcutaneous injection of the suspension of 5×10^6 viable cells (MDA-MB-468, TNBC cell line) under aseptic conditions at the abdominal mammary gland and flanks. Cell injection utilized a 1mL syringe and hypodermic needle 36G [16,17].

The clinical evaluation investigated treatment impacts, considering general physical aspects, behavior, weight, and tumor growth, during the experimental period. Animal weight measurements were made on a digital scale (Toledo 9094), determining weight varies according to tumor progression and performed treatment response. Tumor growth was monitored to assess treatment efficiency. Tumor diameter progression was measured by a high-precision digital caliper (200 mm Mitutoyo 500-172-30B 0.01 mm) [18,19]. Food and water were offered *ad libitum*. However, they were measured for behavior monitoring purposes only.

2.3. Drugs administration and photodynamic therapy

Fourteen weeks after xenograft was established, specific drugs were administrated to animals, according to groups. Saline solution 0,9% was administrated to Group Saline. Meanwhile, Chlorin e6 (2 mg/kg) (19660-77-6, Frontier Scientific), diluted as manufacturer protocol, was administrated to Group Ce6. Finally, BN (2 mg/kg) synthesized were administrated to Groups BN and BN+PDT.

Synthesis of BN was performed based on the methodology described by our group [20]. Concisely, AuNPs were synthesized by conventional sodium citrate reduction of gold chloride method, producing ~21 nm diameter AuNPs. Ce6-cysteamine and EGF-α-lipoic acid complexes were developed using carbodiimide chemistry to link carboxylic acids to primary amines. Therefore, complexes produced were functionalized to AuNPs incubating samples in constant agitation for 48 h. Stable bifunctional nanoprobes developed according to this protocol were purified and stored at 4 °C in the dark.

For the procedure, animals were anesthetized with ketamine (10 mg/kg) and xylazine (80 mg/kg). Drugs were administrated, according to each specific group, through a caudal vein. Drug injection utilized a 1 mL syringe and hypodermic needle 36G. The Photodynamic therapy was executed in animals four hours after drug administration. For treatment, local tissue was irradiated using an energy density of 100 J/cm^2 by a diode laser of 670 nm connected to an optical fiber diffuser (QuantumTech®, São Carlos, Brazil) at a fluency rate of 100 mW/cm [21,22]. All animals were euthanized 48 h after treatment by an overdose of ketamine and xylazine.

The samples were collected with a scalpel, sectioning the entire tumor area. Then, the samples were allocated to a container with buffered 10% formalin until processing according to posterior tests. The samples are submerged in formalin to protect the tissue from being analyzed, preserving cell components. All processes were described by schematic on Fig. 1.

2.4. Leukocyte differential and histological processing

After blood collection from the mice's tail vein, a blood smear was taken to observe hematological differences between the groups. For this, the panoptic fast staining technique was used. The panoptic fast staining technique is a hematological and differential immersion method performed on dead cells to incorporate cells with pink and blue stains, after fixation. The fixation step uses methanol to maintain the cell structures unaltered. The pink stain step uses eosin to dye cell cytoplasm. The blue stain step uses azure B to dye nucleic acids and granules. The staining was performed with the slides immersed in each of the reagents for a short time. After this process, the slides were gently washed with running water to remove stain residues. After drying at room temperature, the slides were observed under an optical microscope to obtain the leukocyte differential, that is, the percentage of each type of leukocyte present on the slides.

For the histological processing, after tissue fixation in formalin, the samples were dehydrated in ethanol solutions (70% to 100%). Xylol was then applied to make the paraffin able to impregnate the tissue. The tissue impregnation with molten paraffin (56–60 °C) eliminates the xylol contained in the material and guarantees total penetration into the gaps left by water and fat, previously presented. This process also facilitates tissue hardening, after cooling, for microtome cuts. The molten paraffin was used to put the tumors in blocks and form molds for the microtomy. Four-μm-thick sections were obtained with a semi-automatic microtome and were stained with hematoxylin/eosin that allowed the visualization of all cellular components.

2.5. Gene expression analysis

For the RNA extraction, the samples were submitted to maceration in a crucible with a ceramic pistil in liquid nitrogen, transferred to a

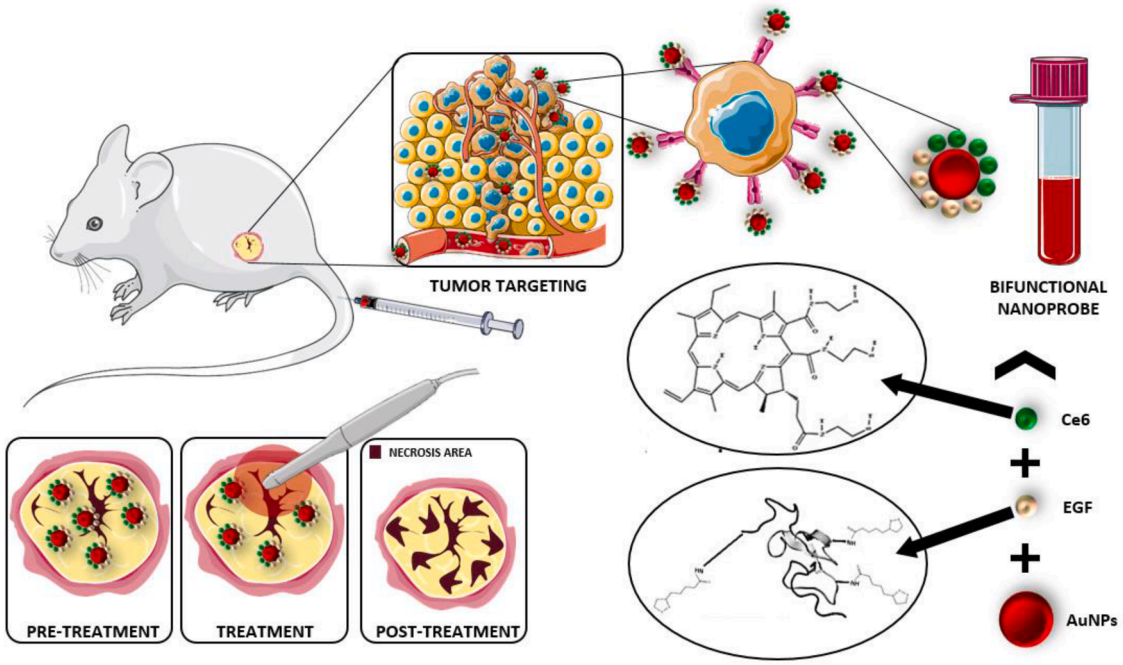

Fig. 1. – Schematic of the bifunctional nanoprobes system studied.

solution of Trizol and chloroform. They were homogenized by vortexing followed by resting for 5 min at room temperature. After this period, the samples were centrifuged. The supernatant was collected, added with Isopropanol, and kept for a minimum of 16 h at -80 °C. After this period, the samples were centrifuged for pellet sedimentation. The pellet was washed three times with 75% ethanol. The material was resuspended with nuclease-free water.

According to the manufacturer's recommendations, each sample was treated with RQ1® RNase-Free DNase for the DNase treatment (Promega Co., Madison, USA). As a negative control for the presence of residual DNA, the DNase-treated RNA was subjected to a standard qPCR reaction to amplify a 128 bp human globin fragment within a single exon so that only DNA fragments could be amplified. Reactions were carried out with Globin forward 5′-GCTTCTGACACAACTGTGTTCAC-3′, Globin reverse 5′-GGCCTCACCACCAACTTCAT-3′ primers at a final concentration of 150 nM in 1x GoTaq® qPCR Master Mix (Promega Co., Madison, USA) in a final volume of 12.5 uL/reaction. The assay was performed on the 7500 Real-Time PCR Systems instrument (Applied Biosystems, California, USA). There was no amplification in any of the samples confirming the effectiveness of the DNase treatment.

For Reverse Transcript followed by qPCR (RT-qPCR), the samples' RNA concentrations were verified by spectrophotometry using NanoDrop2000® (Thermo Scientific, Wilmington, DE), 1ug of RNA followed for reverse transcription using the ImProm-II™ Reverse Transcription System (Promega Co., Madison, USA). The cDNA was then diluted 100X and used for qPCR reactions using specific primers for Bcl-2 (Forward 5′-GGTGGGGTCATGTGTGTGG -3′ Reverse 5′-CGGTTCAGGTACTCAGTCATCC-3′), Bax (Forward 5′-CCCGAGAGGTCTTTTTCCGAG -3′ Reverse 5′- CCAGCCCATGATGGTTCTGAT -3′), Caspase 3 (Forward 5′-CATGGAAGCGAATCAATGGACT -3′ Reverse 5′-CTGTACCAGACCGAGATGTCA -3′), Caspase 8 (Forward 5′-AGAGTCTGTGCCCAAATCAAC -3′ Reverse 5′- GCTGCTTCTCTCTTTGCTGAA-3′), SOD2 (Forward 5′-TGAACAACCTGAACGTCACC-3′ Reverse 5′-GTAGTAAGCGTGCTCCCACA-3′), and Stratifine (14-3-3 - Forward 5′-AAGACCACTTTCGACGAGGC-3′ Reverse 5′-CTCTTCCCCGGCGTTGT-3′). To determine the reference gene, a panel of 8 endogenous genes was used (HPRT1, RPLP0, RPL27, TBP, ACTB, TUBA, GAPDH, and HMBS), and the chosen gene was GAPDH as it had a variation <1 Ct among all samples. From then on, the assays were performed in duplicate using 150nM of each primer in a final reaction of 1x GoTaq® qPCR Master Mix in a final volume of 12.5 uL/reaction in the 7500 Real-Time PCR Systems equipment (Applied Biosystems, California, USA). The reaction conditions were 95 °C for two minutes followed by 40 cycles of 95 °C for 15 s and 60 °C for 1 min. Gene expression analysis was performed using the ΔΔCt1 methodology in which samples are normalized by the reference gene (endogenous) and compared with experimental control samples. The results were then plotted on an Excel spreadsheet and standard deviations determined. Each assay was repeated three times with no significant deviation for each gene tested.

2.6. Statistical analysis

The data are presented as means ± SD, as noted in each case. All values of n are provided. For comparisons between the data sets, One-Way ANOVA and Tukey tests were used. $P < 0.05$ was considered to indicate a statistically significant difference.

3. Results

3.1. Animal clinical evaluation

Body weight was monitored before and during treatment. The change in tumor volume was measured twice a week and after treatment for 15 days (Fig. 2). The mean weight of mice was monitored throughout the entire experiment. Compared with the Saline group, the Ce6+PDT group and the BN+PDT group did not significantly differ in weight, even after PDT. All groups showed significant weight gain in the weeks analyzed, demonstrating that it did not have substantial systemic toxicities but showed antitumor effects.

3.2. BN antitumor effect in vivo associated with PDT

The excellent efficiency of BN after PDT *in vitro*, with active targeting and absorption effect for MDA-MB-468 cells, led to the study of PDT treatment in Balb/c nude mice. After intravenous doses of free Ce6 and BN were administered to mice, the tumor was exposed to irradiation once. As shown in Fig. 3a, the tumor volume was not reduced after irradiation in mice administered with BN. Still, crusting and necrosis

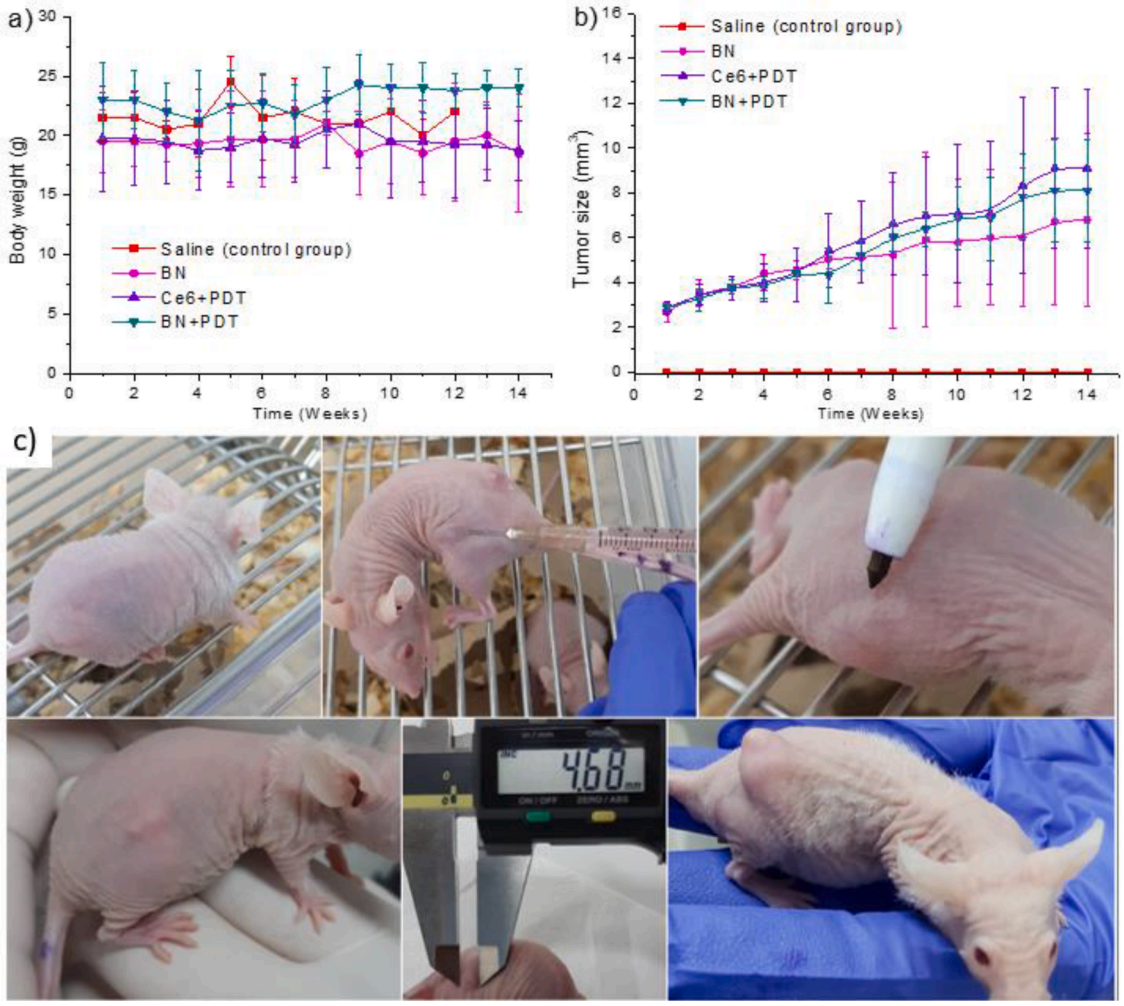

Fig. 2. – Animal clinical evaluation. (a) Changes in body weight monitored over weeks in mice treated as indicated. (b) Changes in tumor volume over time were assessed in mice treated as indicated. The red square, pink circle, purple triangle, and green triangle represent the saline (control group), BN, Ce6+PDT, and BN+PDT groups, respectively. Data are expressed as means ± SD. (c) Scheme of growing tumor: mice before any procedure, mice in xenograft, mice with a papule after xenograft, first signs of a tumor, tumor measuring, and final tumor in 10mm; from left to right (For interpretation of the references to color in this figure legend, the reader is referred to the web version of this article).

could be found on the tumor surface, indicating the efficacy of PDT.

As expected, the *in vivo* experiment results indicated that BN+PDT has a superior therapeutic effect compared to other therapies. In the *in vivo* study, we also confirmed that this concentration performs better than Ce6+PDT, indicating its effect, suggesting that the association with chemotherapy or radiotherapy will have better efficacy. The treatment procedure of the groups is shown in Fig. 3a. The tumor size in each group after treatment is illustrated in Fig. 3c, in which the BN+PDT treatment group exhibits the major necrosis area among all (data presented in 3.5). Tumor volume in the BN+PDT group showed a reduction compared to the BN and Ce6+PDT groups. It is observed that the body weights of all groups of animals were measured, and no detectable weight loss was observed due to the treatments (Fig. 2a).

3.3. BN toxicity in mice

Whole blood samples were obtained from mice of all groups on the day of euthanasia (15 days) to assess changes in leukocyte counts (Fig. 4). The leukocyte counts in the saline group (control group) mice were significantly different from the free Ce6+PDT and BN+PDT group ($P > 0.05$, One-Way ANOVA, Tukey Test). BALB/c nude mice resisted the application injected intravenously into mice 2 ug/ml of BN and free Ce6 were analyzed for 15 days and showed no signs of toxicity. In addition, we did not find lymphopenia in mice, and no alteration was identified in the white blood cell count ($P = 0.65$, One-Way ANOVA, Tukey Test) (Fig. 4).

3.4. Tumor histopathological classification

After treatment, H&E staining of tumor tissues showed the tissue became smaller and pyknotic, and the intracellular chromatin content markedly decreased. The relative fraction of death/live cells increased in the following order: Saline, BN, Ce6+PDT, and BN+PDT. The histological analysis allowed to classify the tumors developed into better differentiated invasive breast carcinoma, characterized by epithelial cells. In all samples, in the BN group and groups treated with PDT (Fig. 5), several malignancy characteristics were observed, such as evident nucleoli, atypical mitosis, inflammatory infiltrate, increase in tumor cell clusters, characteristic of tissue tumor mammary Fig. 5.a represents the tumor and photomicrographs of the BN group. A set of neoplastic cells is observed, mainly forming the periphery of the tumor. This cell cluster presents itself with both cellular cords and the appearance of “blocks” of cells. This cords or blocks of neoplastic cells are in the middle of dense fibrous tissue and present an increased nuclear basophilia, meaning that this group is characterized by a severe desmoplastic reaction of the infiltrated tumor tissue. This reaction is also

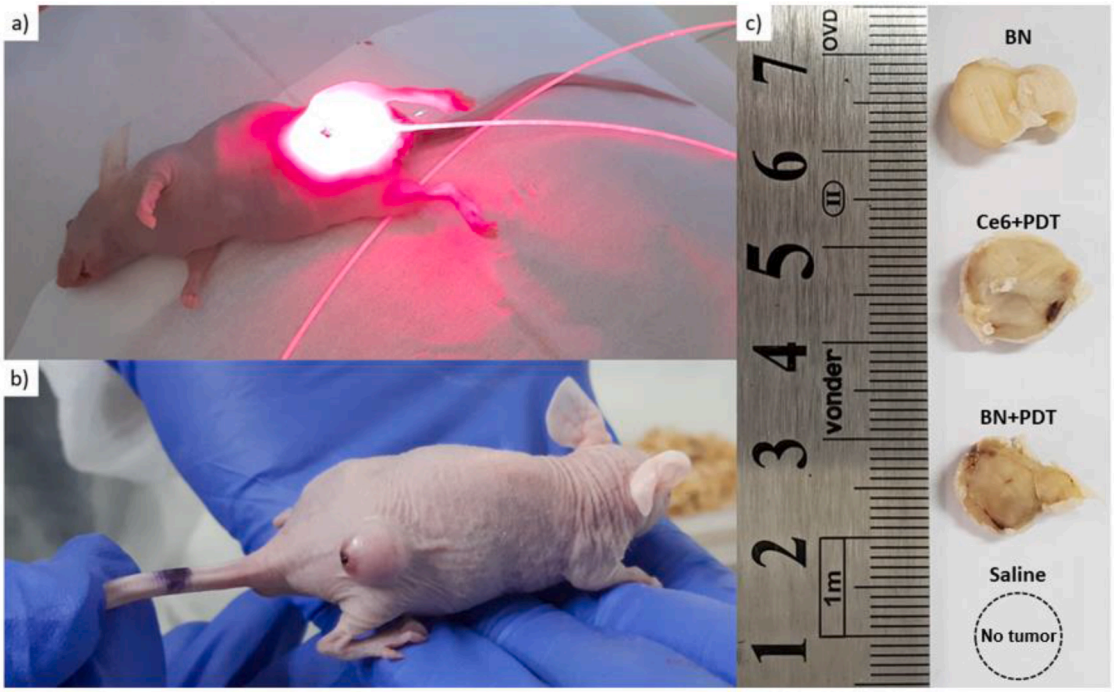

Fig. 3. - Combination of PDT to treat MDA-MB-468 tumor xenograft mice: (a) The laser was conducted on xenografted mice under *in vivo* conditions, irradiation with a 670 nm laser for PDT was applied for 10 min, 4 h later the drug injection. (b) Necrosis after exposure to PDT. (c) tumors after treatment on a scale expressed in centimeters and millimeters.

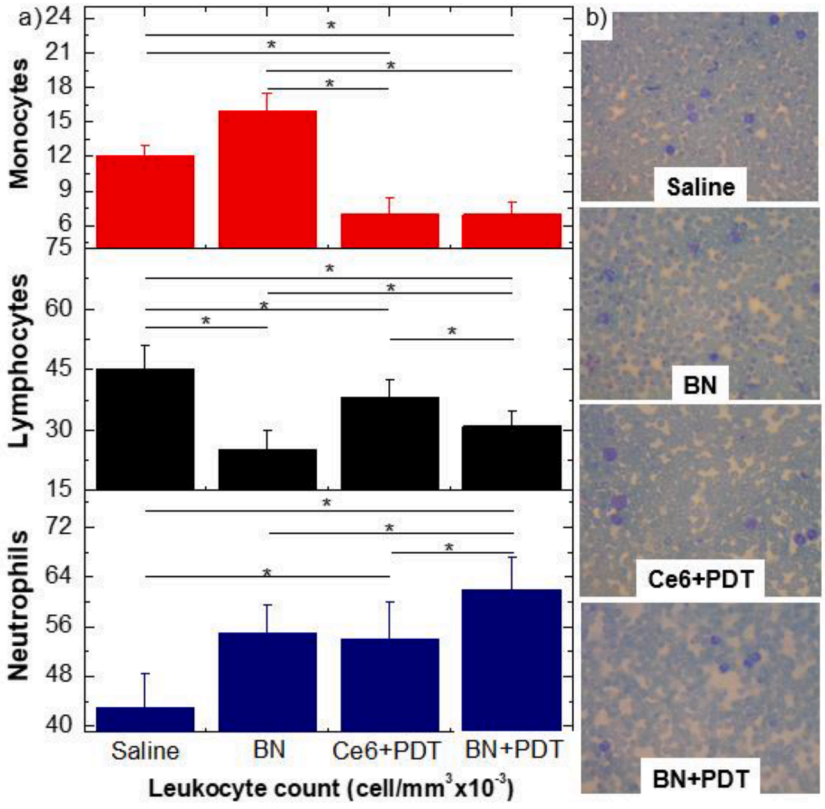

Fig. 4. - Blood samples collected from the tail vein of BALB/c nude mice from all groups. (a) The leukocyte type fraction was determined by microscopic examination of Panoptic Rapid stained peripheral blood smears and expressed as a percentage. The graphic represents the mean values of total leukocyte count in each group. Values are means ± SD ($p < 0.05$ by One-Way ANOVA, Tukey Test). Each experiment was performed in triplicates. (b) representative photomicrographs of saline, BN, Ce6+PDT and BN+PDT groups after PDT treatment.

observed in the central region of the tumor, among some areas of necrosis, which are characterized by an acidophilic area, presence of some cell fragments, and with a "shadow" of neoplastic cells.

Fig. 5b represents the tumor and photomicrographs of the Ce6+PDT group. A cluster of neoplastic cells is also observed in the tumor periphery, with the same morphological appearance as the cells in the untreated group and in the middle of fibrous tissue. However, this desmoplastic reaction of the infiltrated tumor tissue occupies a lesser

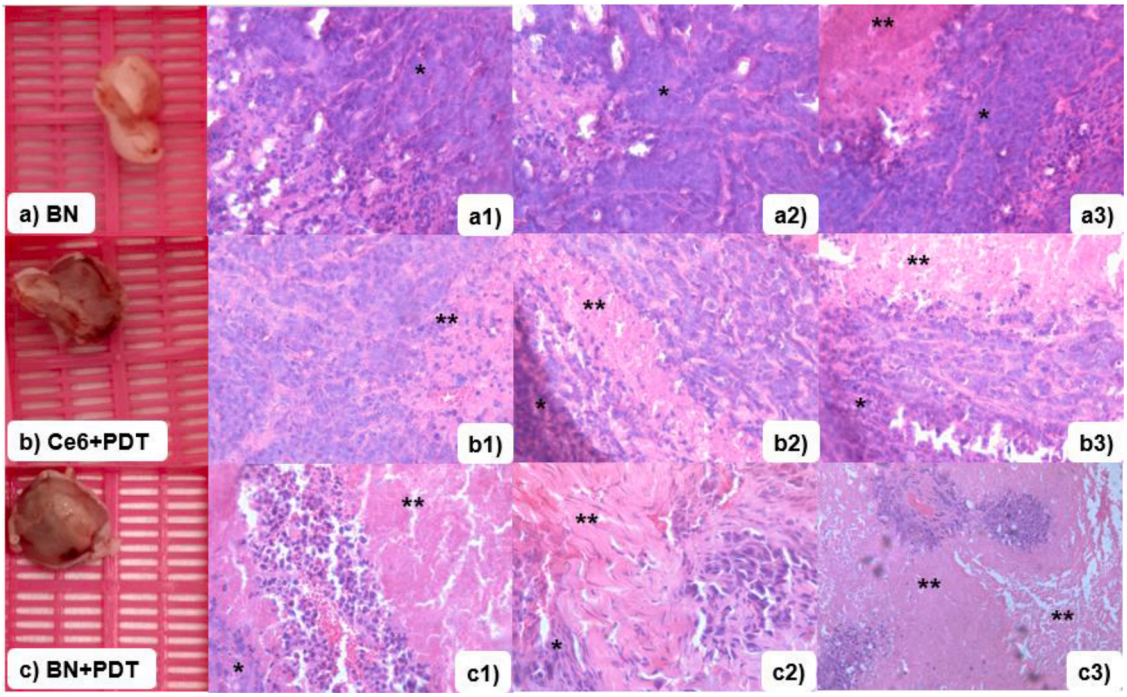

Fig. 5. - Histological analyses of the MDA-MB-468 breast tumor model. Tissues were harvested 48 h after photodynamic therapy. This figure presents the image of a breast cancer model removed from mice and their result of H&E staining; (a) Group BN, a severe desmoplastic reaction of the infiltrated tumor tissue is observed, mainly forming the periphery of the tumor and in the central region of the tumor, among some areas of necrosis; (b) Group Ce6+PDT, a moderate desmoplastic reaction occupies a lesser extent than in the untreated group, and more necrotic areas are observed; (c) Group BN+PDT, the desmoplastic reaction is restricted only to the periphery of the tumor. Necrotic areas occupy the most part of tumor, which has small or no cell fragments. Compared with tissues in the BN group, those in the BN+PDT group showed cell and nuclear damage. * desmoplastic reaction; ** area of necrosis. H&E staining with a magnification of 20x.

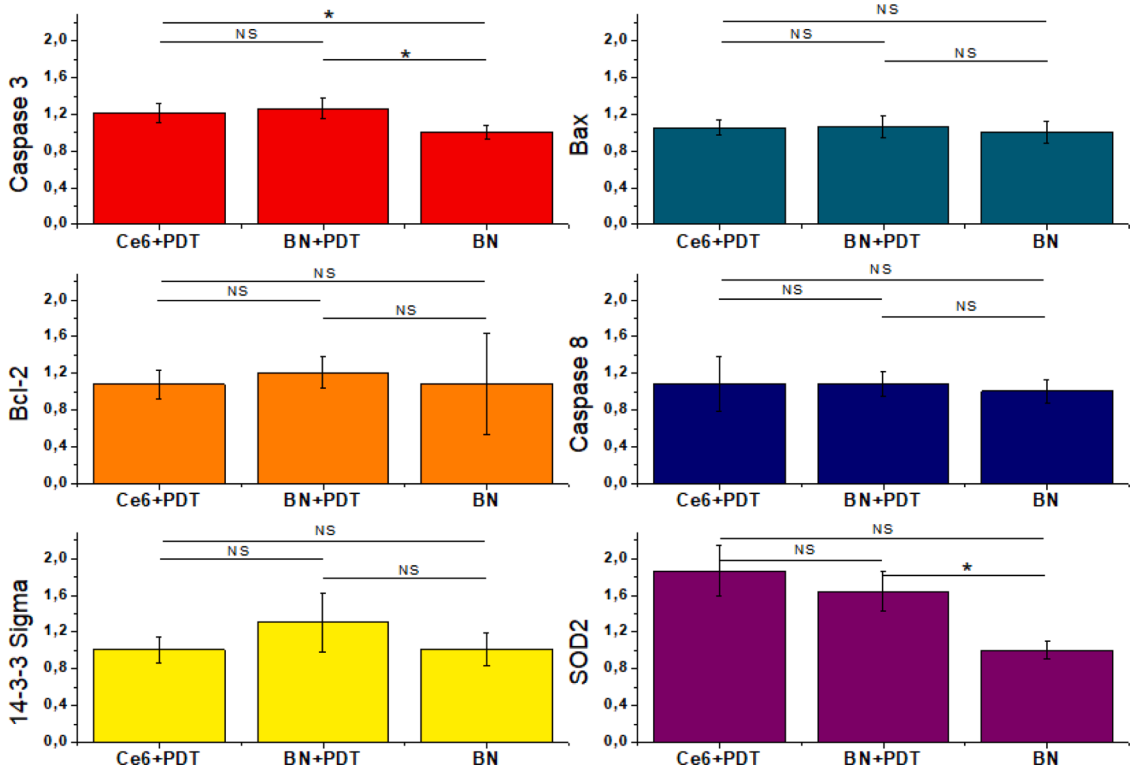

Fig. 6. - Reverse transcription-quantitative PCR analysis of *Bax, Bcl-2, Caspase 3* e *Caspase 8, SOD2, 14-3-3 sigma* gene expression in TNBC xenograft. Statistical analysis was performed using the Singleplex test. Data were normalized by GAPDH expression level. Bars represent standard deviations. The expression level was higher in BN+PDT samples compared with Ce6+PDT and BN groups. * - Significant difference. NS - Non significant.

extent when compared to the untreated group. In addition, most of the cells are dysmorphic, with smaller nuclei, no evident nucleoli, with a slight bluish coloration, together with cell fragments amidst the fibrous tissue. These characteristics intensify close to the central region of the tumor. Likewise, more significant areas of necrosis are observed in this group when compared to the untreated group.

Fig. 5c represents the tumor and photomicrographs of the BN+PDT group. In this group, the desmoplastic reaction is restricted only to the tumor periphery. Most of the tumor is composed of an extensive areas of necrosis, some of them with small cell fragments with intense basophilia. In addition, based on the staining images, the group treated with BN+PDT showed the most remarkable necrosis and severe morphological change, which also proves the effect is much better than the other groups. H&E staining identified that the tumor in the BN+PDT group was significantly suppressed compared to the BN and Ce6+PDT group (Fig. 5c). These results demonstrated that BN+PDT could effectively inhibit tumors under laser irradiation with low side effects.

3.5. Analysis of apoptotic proteins expression

As the *in vivo* experiments showed that the best results belonged to the BN+ PDT group, the expression of some apoptotic proteins was analyzed. Real-time PCR data demonstrated that the expression of pro-apoptotic proteins *Bax, Bcl-2, Caspase 3* and *Caspase 8, SOD2,* and *14-3-3 sigma* were significantly higher in the BN+PDT group compared to the control, indicative of apoptosis induction in this group (Fig. 6). They show a 20% and 27% increase in *caspase 3* expression (Ce6+PDT and BN+PDT, respectively) and a 20% increase in *Bcl-2* expression in BN+PDT treatment. Additionally, two genes related to DNA damage and oxidative stress (*14-3-3 sigma* and *SOD2*) were analyzed, resulting in a 30% increase of *14-3-3 sigma* in BN+PDT and 84% and 64 % for the *SOD2* gene with the treatments Ce6+PDT and BN+PDT, respectively.

4. Discussion

In the present study, we proposed the PDT protocol for the treatment of triple-negative breast cancer. BN was produced to improve free Ce6 action through functionalization with AuNPs. High hydrophobic characteristic of Ce6 facilitates the formation of aggregates in an aqueous solution, preventing the production of $^1O_2$. Hydrophobicity hinders solubility in physiological solvents and body fluids, making its clinical application impossible. Co-binding of EGF has been used to increase selectivity and colloidal stability as determined in previous studies [23]. Due to the limitations of using PDT alone to treat breast cancer, the association of nanoparticles was considered a favorable solution. Thus, in the present study, we immobilized Ce6 as a photosensitizing reagent in the AuNPs nanocarrier to treat breast cancer *in vivo*.

For *in vivo* analysis, we evaluated three treatment groups, including control, Ce6+PDT, and BN+PDT. In our leading treatment group (BN+PDT), Ce6 functioned like PS, activated by red laser, and produced singlet oxygen. BN was injected into the mouse model with TNBC, followed by ordered red laser irradiation. *In vivo* results indicated that the xenografts had a progressive growth throughout the follow-up period. Mean tumor volume reached 10 mm^3 at the end of the treatment considering its initial volume.

Our data showed that treatment with free Ce6+PDT and BN+PDT reduced tumor volume compared to the non-irradiated BN group. BN group had a tumor regression of 43%. The effect of BN on tumor volume may be related to the properties of Ce6. In PDT approach, excitation of inactive photosensitizers by an appropriate light wavelength leads to ROS production and subsequent apoptosis of tumor cells. Ce6 is related to the class of tetrapyrrolic substances derived from porphyrin. It contains one of its pyrrolic rings in limited form, resulting in the molecule's symmetry and its conjugation. Due to its Q band shift presents absorption in the red region in the UV-visible spectrum [24,25].

These data correspond to the results observed in the present study, in which Ce6 loaded in NPs from AuNPs dissociated easily in tumors compared to free Ce6. One of the limitations of PDT is its oxygen-scavenging property since tumor cells need adequate PS absorption. Some studies have reported an increase in membrane permeability and cellular uptake of several anti-cancer PSs, due to the use of laser in PDT [26]. Laser association can increase the oscillation potential that generates an absorption increase of NPs radiation. This phenomenon occurs in visible region, showing that free electrons oscillate on metallic surface, in surface plasmonic resonance. Demonstrating that they can be used in chemical, biological, and nanotechnology applications, enabling the permeability and retention effect to target the tumor via treatment with the BN+PDT approach, confirming the previous data [27,28]. In our study, surface functionalization of AuNPs with EGFR enabled the drug to be effectively transported to the tumor for irradiation [29].

Furthermore, the biocompatible surface coating can be added to the AuNP surface to enable applications in the biomedical area [30]. In AuNP-mediated PDT, BNs can be delivered with active targeting, followed by ROS production and tumor destruction. As an example, approaching a study in our group using carbodiimide chemistry, Ce6 was covalently bound to thiourea and (through the final sulfur group) to gold nanoparticles (AuNPs), forming the Ce6-AuNP complex. When irradiated at 660 nm, the cytotoxicity of Ce6-AuNP was more significant than free Ce6 for MDA-MB-468 cells *in vitro* [31]. In another approach, a study that used PDT in skin squamous cell tumor treatments investigated gold nanoparticles conjugation (GNPs) to 5-aminolevulinic acid (5-ALA), concluding that the results suggested that the conjugate significantly increased the antitumor efficacy of PDT in A431 cells [32]. Some authors have evaluated mice with subcutaneous tumors receiving gold nanoparticles targeted to epidermal growth factor peptides (EGF-pep-AuNPs) followed by laser irradiation at 672 nm, suggesting a reduction in volume observed in treated tumors, selectively activated with light [33]. In the present study, tumor volume in the BN+PDT group showed more than 78% reduction compared to the other treatment groups. Also, note that this BN+PDT treatment group achieved less tumor volume than the initial volume. This significant reduction in tumor volume could be explained by ROS production in tumor by PDT.

Our findings agree with Castilho et al. [20] confirming the results found in this study on the efficacy of combining BN with PDT; for example, AuNPs was designed as the carrier for Ce6 PS where the obtained compound had a suitable solubility to be used in PDT with a better efficacy compared to free Ce6. It is important to remember that EGFR has provided PS delivery to tumor cells [34]. Furthermore, a study with PDT approach showed that AuNPs could produce singlet $1O_2$ due to the therapeutic properties observed in an *in vivo* cancer model [35]. Our data showed that the primary treatment strategy, BN+PDT, effectively suggested tumor regression, possibly due to hypoxia and necrosis in the center. However, in the Ce6+PDT group, it showed less involvement in tumor volume.

PDT can stimulate changes in the plasma membrane; as a result, we observed infiltrates of leukocytes in histological sections. In these sections, neutrophils were prevailing on differential count of leukocytes in tumor after PDT, which presented some significant differences between groups. Therefore, there were no infectious or inflammatory processes, remaining within normal parameters. The representative photomicrographs present blood cells from all groups analyzed. The 2 μl/mL dose was supported in mice. It showed no weakness, visible signs of toxicity and suggests regression of xenograft growth with overexpression of EGFR in BALB/c mice by 58% [36].

Thus, in the mouse hematoxylin and eosin (H&E) experiment, it was observed that the treatment with BN+PDT was related to a more intense loss of tumor tissue when compared to the other treatments. Tumor tissue morphology was significantly modified after treatment with BN+PDT. These findings confirm that BN+PDT had a significant therapeutic effect on tumors.

Based on these arguments, in this study, the quantitative real-time PCR test was used to assess the relative expression of genes related to

apoptosis to provide identification of the pathway affected by PDT treatment in breast tumors from samples obtained *in vivo*. The PCR results revealed that the expression of apoptotic factors including *Bax, Bcl-2, Caspase 3* and *8, SOD2, 14-3-3 Sigma* significantly increased in the BN+PDT group compared to the control group. The expression increase confirms that tumor shrinkage in this group may be associated with the occurrence of apoptosis through mitochondria. As a result, it was shown that PDT and BN increased apoptotic gene expression in breast cancer cells. Thus, in a study, they used MPEG2000-ZIF/PC compositions (PMs) in combination with PDT inducing apoptotic death in tumor cells and observed an increase in the expression level of *Caspase3, Bax*, and *Bcl-2* after PDT [37]. Also, one study reported that they used Dihydroartemisinin (DHA) in combination with PDT to inhibit breast cancer cell proliferation and increased expression of the *caspase 8* protein, suggesting that it may activate *caspase 3* [38]. In another report, the study used zinc phthalocyanine (M2TG3) associated with PDT to treat different tumors and observed that M2TG3 could cause cell death via several mechanisms, depending on the condition of cell cultures, model, and oxygen availability, revealed that hypoxia increased the level of superoxide dismutase (*SOD2*) [39]. Furthermore, reports of a study with the 14-3-3 protein showing that its association with the proliferation of tumor cells and apoptosis indicates its presence in cancer with a worse prognosis [40]. Therefore, it is noteworthy that no side effects resulting from the treatment technique in mice were identified, which is an advantage compared to some conventional therapies such as chemotherapy.

5. Conclusion

Aiming to produce a drug that overcomes all challenges during drug delivery, we present the application of coated gold nanoparticles for breast cancer therapy *in vivo*. The study showed promising development of an innovative method to breast cancer treatment. Nanoprobes provided a targeting effect on potential drug delivery to the tumor, exhibiting biocompatibility evaluated by leukocyte count analysis. This analysis showed tumor regression due to tissue damage caused by PDT, such as necrosis and/or apoptosis. Tissue damage and tumor regression were evaluated by histopathological analysis and RT-qPCR, which determined the changes promoted in the markers that regulate tumor regression, showing increased expression of apoptotic factors (Bax, Bcl-2, Caspase 3 and 8, SOD2, 14-3-3 Sigma), in PDT+BN treated group showing greater involvement. Therefore, aiming at the need for new technologies against breast cancer, we studied a less invasive and with fewer side effects treatment.

CRediT authorship contribution statement

Viviane Paula dos Santos Jesus: Writing – original draft, Visualization, Methodology, Validation, Investigation, Formal analysis, Conceptualization, Data curation. **Paula Fonseca Antunes Vieira:** Formal analysis, Investigation, Methodology, Visualization, Writing – review & editing. **Ricardo Cesar Cintra:** Writing – review & editing, Methodology. **Luciana Barros Sant'Anna:** Writing – review & editing, Methodology. **Denise Maria Zezell:** Writing – review & editing, Investigation. **Maiara Lima Castilho:** Project administration, Writing – review & editing. **Leandro Raniero:** Writing – review & editing, Supervision, Resources, Project administration, Funding acquisition.

Declaration of Competing Interest

The authors declare that they have no known competing financial interests or personal relationships that could have appeared to influence the work reported in this paper.

Acknowledgments

The authors would like to thank Priscila Leite, technician of Multiuser Laboratory Center of Vale do Paraíba University, for the technical help and the use of bioterium. We would also like to thank the FOTOBIOS lab for the use of equipment. Brazilian agencies CAPES for the Ph. D. scholarships (code 001, process number 8881.361771/2019-01), FAPESP (Project 2017/07519-2), CNPq (302944/2018-4), and FINEP (Conv.01.18.0053.00).

References

[1] S. Sun, et al., Ultrasound-targeted photodynamic and gene dual therapy for effectively inhibiting triple negative breast cancer by cationic porphyrin lipid microbubbles loaded with HIF1α-siRNA, Nanoscale 10 (42) (2018) 19945–19956, https://doi.org/10.1039/C8NR03074J.
[2] A. Gangi, et al., Breast-conserving therapy for triple-negative breast cancer, JAMA Surg. 149 (3) (2014) 252–258, https://doi.org/10.1001/jamasurg.2013.3037.
[3] D.Y. Wang, et al., Molecular stratification within triple-negative breast cancer subtypes, Sci. Rep. 9 (1) (2019) 1–10, https://doi.org/10.1038/s41598-019-55710-w.
[4] A. Santonja, et al., Triple negative breast cancer subtypes and pathologic complete response rate to neoadjuvant chemotherapy, Oncotarget 9 (41) (2018) 26406, https://doi.org/10.18632/oncotarget.25413.
[5] V.G. Abramson, et al., Subtyping of triple-negative breast cancer: implications for therapy, Cancer 121 (1) (2015) 8–16, https://doi.org/10.1002/cncr.28914.
[6] L. Yehia, et al., Expression of HIF-1α and markers of angiogenesis are not significantly different in triple negative breast cancer compared to other breast cancer molecular subtypes: implications for future therapy, PLoS One 10 (6) (2015), e0129356, https://doi.org/10.1371/journal.pone.0129356.
[7] H. Axelson, et al., Hypoxia-induced dedifferentiation of tumor cells–a mechanism behind heterogeneity and aggressiveness of solid tumors. Semin. Cell Dev. Biol., Academic Press, 2005, pp. 554–563, https://doi.org/10.1016/j.semcdb.2005.03.007.
[8] P. Vaupel, L. Harrison, Tumor hypoxia: causative factors, compensatory mechanisms, and cellular response, Oncologist 9 (2004) 4–9, https://doi.org/10.1634/theoncologist.9-90005-4.
[9] T. Nagaya, et al., Near infrared photoimmunotherapy targeting EGFR positive triple negative breast cancer: optimizing the conjugate-light regimen, PLoS One 10 (8) (2015), e0136829, https://doi.org/10.1371/journal.pone.0136829.
[10] F. Bertucci, P. Finetti, D. Birnbaum, Basal breast cancer: a complex and deadly molecular subtype, Curr. Mol. Med. 12 (1) (2012) 96–110, https://doi.org/10.2174/156652412798376134.
[11] P. Huang, et al., Photodynamic treatment with purpurin 18 effectively inhibits triple negative breast cancer by inducing cell apoptosis, Lasers Med. Sci. 36 (2) (2021) 339–347, https://doi.org/10.1007/s10103-020-03035-w.
[12] S. Kwiatkowski, et al., Photodynamic therapy–mechanisms, photosensitizers and combinations, Biomed. Pharmacother. 106 (2018) 1098–1107, https://doi.org/10.1016/j.biopha.2018.07.049.
[13] N.L. Oleinick, H.H. Evans, The photobiology of photodynamic therapy: cellular targets and mechanisms, Radiat. Res. 150 (5s) (1998) S146–S156, https://doi.org/10.2307/3579816.
[14] M. Triesscheijn, et al., Photodynamic therapy in oncology, Oncologist 11 (9) (2006) 1034–1044, https://doi.org/10.1634/theoncologist.11-9-1034.
[15] C. Yue, et al., Near-infrared light triggered ROS-activated theranostic platform based on Ce6-CPT-UCNPs for simultaneous fluorescence imaging and chemo-photodynamic combined therapy, Theranostics 6 (4) (2016) 456, https://doi.org/10.7150/thno.14101.
[16] K.S. Kim, et al., Multifunctional trastuzumab-chlorin e6 conjugate for treatment of HER2-positive human breast cancer, Biomater. Sci. (6) (2018) 1217–1226, https://doi.org/10.1039/C7BM01084B.
[17] M.A. Sarcinelli, et al., Nanoradiopharmaceuticals for breast cancer imaging: development, characterization, and imaging in inducted animals, Onco Targets Ther. 9 (2016) 5847–5854, https://doi.org/10.2147/OTT.S110787.
[18] H. Jeong, et al., Photosensitizer-conjugated human serum albumin nanoparticles for effective photodynamic therapy, Theranostics 1 (2011) 230–239, https://doi.org/10.7150/thno/v01p0230.
[19] M.H. Yazdi, et al., The immunostimulatory effect of biogenic selenium nanoparticles on the 4T1 breast cancer model: an *in vivo* study, Biol. Trace Elem. Res. 149 (2012) 22–28, https://doi.org/10.1007/s12011-012-9402-0.
[20] M.L. Castilho, K.C. Hewitt, L. Raniero, FT-IR characterization of a theranostic nanoprobe for photodynamic therapy and epidermal growth factor receptor targets, Sens. Actuators B 240 (2017) 903–908, https://doi.org/10.1016/j.snb.2016.09.011.
[21] B. Park, et al., Korean risk assessment model for breast cancer risk prediction, PLoS One 8 (2013) e76736, https://doi.org/10.1371/journal.pone.0076736.
[22] I.l. Yoon, et al., Advance in photosensitizers and light delivery for photodynamic therapy, Clin. Endosc. 46 (2013) 7–13, https://doi.org/10.5946/ce.2013.46.1.7.
[23] C.K. Lim, et al., Nanophotosensitizers toward advanced photodynamic therapy of cancer, Cancer Lett. 334 (2) (2013) 176–187, https://doi.org/10.1016/j.canlet.2012.09.012.

[24] M.L. Castilho, V.P. Jesus, P.F. Vieira, K.C. Hewitt, L. Raniero, Chlorin e6-EGF conjugated gold nanoparticles as a nanomedicine based therapeutic agent for triple negative breast cancer, Photodiagn. Photodyn. Ther. 33 (2021), 102186, https://doi.org/10.1016/j.pdpdt.2021.102186.
[25] V. Pérez-Laguna, L. Pérez-Artiaga, V. Lampaya-Pérez, S.C. López, I. García-Luque, M.J. Revillo, et al., Comparative effect of photodynamic therapy on separated or mixed cultures of Streptococcus mutans and Streptococcus sanguinis, Photodiagn. Photodyn. Ther. 19 (2017) 98–102, https://doi.org/10.1016/j.pdpdt.2017.05.017.
[26] D. Xu, et al., Multifunctional nanoparticle PEG-Ce6-Gd for MRI-guided photodynamic therapy, Oncol. Rep. 45 (2) (2021) 547–556, https://doi.org/10.3892/or.2020.7871.
[27] X. Huang, et al., Cancer cell imaging and photothermal therapy in the near-infrared region by using gold nanorods, J. Am. Chem. Soc. 128 (6) (2006) 2115–2120, https://doi.org/10.1021/ja057254a.
[28] M.C. Daniel, D. Astruc, Gold nanoparticles: assembly, supramolecular chemistry, quantum-size-related properties, and applications toward biology, catalysis, and nanotechnology, Chem. Rev. 104 (1) (2004) 293–346, https://doi.org/10.1021/cr030698+.
[29] S. Siddique, J.C.L. Chow, Gold nanoparticles for drug delivery and cancer therapy, Appl. Sci. 10 (11) (2020) 3824, https://doi.org/10.3390/app10113824.
[30] D. Nozdriukhin, et al., Gold nanoparticle-carbon nanotube multilayers on silica microspheres: optoacoustic-Raman enhancement and potential biomedical applications, Mater. Sci. Eng. C 120 (2021), 111736, https://doi.org/10.1016/j.msec.2020.111736.
[31] L. Vieira, M.L. Castilho, I. Ferreira, J. Ferreira-Strixino, K.C. Hewitt, L. Raniero, Synthesis and characterization of gold nanostructured Chorin e6 for photodynamic therapy, Photodiagn. Photodyn. Ther. 18 (2017) 6–11, https://doi.org/10.1016/j.pdpdt.2016.12.012.
[32] Y.F. Chi, J.J. Qin, Z. Li, Q. Ge, W.H. Zeng, Enhanced anti-tumor efficacy of 5-aminolevulinic acid-gold nanoparticles-mediated photodynamic therapy in cutaneous squamous cell carcinoma cells, Braz. J. Med. Biol. Res. 53 (2020), https://doi.org/10.1590/1414-431X20208457.
[33] J.D. Meyers, Y. Cheng, A.M. Broome, R.S. Agnes, M.D. Schluchter, S. Margevicius, J.P. Basilion, Peptide-targeted gold nanoparticles for photodynamic therapy of brain cancer, Part. Part. Syst. Charact. 32 (4) (2015) 448–457, https://doi.org/10.1002/ppsc.201400119.
[34] M.H. Chang, C.L. Pai, Y.C. Chen, H.P. Yu, C.Y. Hsu, P.S. Lai, Enhanced antitumor effects of epidermal growth factor receptor targetable cetuximab-conjugated polymeric micelles for photodynamic therapy, Nanomaterials 8 (2) (2018) 121, https://doi.org/10.3390/nano8020121 (Basel, Switzerland).
[35] P.G. Calavia, G. Bruce, L. Pérez-García, D.A. Russell, Photosensitiser-gold nanoparticle conjugates for photodynamic therapy of cancer, Photochem. Photobiol. Sci. 17 (11) (2018) 1534–1552, https://doi.org/10.1039/C8PP00271A.
[36] S.O. Gollnick, S.S. Evans, H. Baumann, B. Owczarczak, P. Maier, L. Vaughan, B. W. Henderson, Role of cytokines in photodynamic therapy-induced local and systemic inflammation, Br. J. Cancer 88 (11) (2003) 1772–1779, https://doi.org/10.1038/sj.bjc.6600864.
[37] D. Chen, M. Suo, J. Guo, W. Tang, W. Jiang, Y. Liu, Y. Duo, Development of MOF "Armor-Plated" phycocyanin and synergistic inhibition of cellular respiration for hypoxic photodynamic therapy in patient-derived xenograft models, Adv. Healthc. Mater. 10 (3) (2021), 2001577, https://doi.org/10.1002/adhm.202001577.
[38] X. Dai, X. Zhang, W. Chen, Y. Chen, Q. Zhang, S. Mo, J. Lu, Dihydroartemisinin: a potential natural anticancer drug, Int. J. Biol. Sci. 17 (2) (2021) 603–622, https://doi.org/10.7150/ijbs.50364.
[39] M. Kucinska, A. Plewinski, W. Szczolko, M. Kaczmarek, T. Goslinski, M. Murias, Modeling the photodynamic effect in 2D versus 3D cell culture under normoxic and hypoxic conditions, Free Radic. Biol. Med. 162 (2021) 309–326, https://doi.org/10.1016/j.freeradbiomed.2020.10.304.
[40] N. Li, H. Wang, J. Fan, C. Tong, J. Yang, H. Wei, R. Ling, Overexpression of 14-3-3θ promotes tumor metastasis and indicates poor prognosis in breast carcinoma, Oncotarget 5 (1) (2014) 249, https://doi.org/10.18632/oncotarget.1502.